Quantum interferences between rescattering orbits with multiexcitation channels in the recollision excitation process of nonsequential double ionization

Yuna Yang,[1,2] Mingqing Liu,[1] Xiaolei Hao,[3,*] and Jing Chen[1,4,†]

[1]*Institute of Applied Physics and Computational Mathematics, Beijing 100088, China*

[2]*College of Science, Tianjin University of Technology, Tianjin 300384, China*

[3]*Institute of Theoretical Physics and Department of Physics, State Key Laboratory of Quantum Optics and Quantum Optics Devices,Collaborative Innovation Center of Extreme Optics, Shanxi University, Taiyuan 030006, China*

[4]*Center for Advanced Material Diagnostic Technology, Shenzhen Technology University, Shenzhen 518118, China*

(Received 6 January 2021; accepted 26 February 2021; published 18 March 2021)

Based on the strong-field approximation (SFA), we investigate the interference between different returning orbits of the rescattering electron in nonsequential double ionization. We find that the effect of interference is negligible in the recollision-impact ionization process but is prominent in the recollision excitation with subsequent ionization process and induces fast oscillation with constant period in the laser intensity dependence of the asymmetry parameter. The dominant contribution to the fast oscillation comes from the mixed interference between different pairs of returning orbits in different excitation channels. However, the oscillation disappears after laser focus averaging is performed due to its rather small period.

DOI: 10.1103/PhysRevA.103.033111

I. INTRODUCTION

Nonsequential double ionization (NSDI) in strong laser fields has been continuously attracting growing attention from researchers because it is an ideal system to study multielectron dynamics, particularly electron correlation in external fields [1–10]. Rescattering has already been widely accepted as the dominant mechanism [11–14] for NSDI. During the rescattering process, the first electron ionized by tunneling may then be driven back by the laser field with significant kinetic energy and collide with the core inelastically. Depending on the kinetic-energy transferred to the core upon collision, the second electron can be ionized through two mechanisms: (a) to be ionized directly (recollision-impact ionization: RII); or (b) to be excited and subsequently freed by the field (recollision excitation with subsequent ionization: RESI).

In a laser field whose intensity is below the RII threshold, i.e., the maximal returning kinetic energy of the first electron is smaller than the ionization potential, the RESI process will play a dominant role [15–18]. Since RESI is essentially a quantum process, quantum interference plays an important role in it. Up to now, there are mainly three types of interference that are widely identified theoretically and employed to explain experimental results: (a) interference between different excitation channels of the second electron [19]; (b) intracycle and intercycle interference for orbits of the second electron after tunneling ionization [20]; and (c) interference induced by the exchange symmetry for the two ionized electrons which are indistinguishable in nature [20,21]. These interferences have been intensively studied in theory and can be employed to explain many experimental results. For instance, investigation in RESI of Ar by strong-field approximation (SFA) supports pronounced interchannel interference among three identified dominant channels [19], and qualitatively reproduces the measured transition of electron momentum correlation distribution from anticorrelation to correlation with increasing laser intensity [9]. Interference between orbits of the second electron after ionization and interference due to electron indistinguishability also form rich distribution patterns of electron momentum correlation distribution [20]. Furthermore, the interplay between symmetry-related interference and interchannel interference can be manipulated to generate dramatic variations in the shape of momentum correlation distribution [22]. Nevertheless, there are still features observed in experiments concerning RESI that can hardly be attributed to the above interferences. For example, it is found experimentally that the intensity dependence of the asymmetry parameter between the yields in the second and fourth quadrants and those in the first and third quadrants of the electron-momentum-correlation distributions for Xe exhibits a peculiar fast oscillatory structure [23]. The envelope of the oscillation structure can be reproduced by SFA calculation when interchannel interference is taken into account, while the fast oscillation itself cannot be interpreted by either type of the above interference.

Actually, there is another interference between orbits of rescattering electron which plays an important role in processes of above-threshold ionization (ATI) and high-order-harmonic generation (HHG). For example, the resonance-like enhancement structure [24,25] in high-order ATI spectrum can be attributed to constructive interference of a large number of rescattering electronic trajectories with small momenta which happens near channel closings [26–29]. And interference between short and long electronic trajectories will lead

*xlhao@sxu.edu.cn

†chen_jing@iapcm.ac.cn

to an inner region with long coherence time and an outer one with short coherence time in the HHG spectrum [30]. For NSDI, there are only a few investigations on this type of interference. The relevant research involves theoretical observations of resonant-like enhancements of RII for Xe due to the interference of rescattering trajectories with long travel times [31], and the momentum distribution pattern of RESI for He induced by interference between long and short trajectories in one pair with the shortest travel time [20]. But there is no experimental evidence for them up to now.

In this paper, we explore the interferences between returning orbits of the first electron in the RESI process and try to interpret the measured fast oscillation structures. Specifically, we employ SFA theory [19] to calculate the electron momentum correlation distribution and the laser intensity dependence of asymmetry parameter under scenarios with different interferences considered.

The rest of this paper is organized as follows: In Sec. II we briefly recall the expression for the RII and RESI transition amplitude and the saddle-point equations. In Sec. III, we calculate the intensity-dependent electron momentum correlation distribution and asymmetry parameter considering different types of interferences to analyze the effects of interferences between rescattering electron orbits. Finally, in Sec. IV we state the main conclusions of the paper.

II. THEORETICAL METHOD

In our work, we use the S-matrix theory to investigate the electron momentum correlation distribution of the RII process and the RESI process for Xe. Our calculations are based on the velocity-gauge strong-field approximation. The transition amplitude of the RII process is

$$M^{RII}(\mathbf{p}_1,\mathbf{p}_2)=\int_{-\infty}^{\infty}dt'\int_{-\infty}^{t'}dt''\int d^3\mathbf{k}V_{\mathbf{p}_1\mathbf{p}_2,\mathbf{k}g}V_{\mathbf{k}g}e^{iS(\mathbf{p}_1,\mathbf{p}_2,\mathbf{k},t',t'')}, \tag{1}$$

with the action

$$\begin{aligned}S(\mathbf{p}_1,\mathbf{p}_2,\mathbf{k},t',t'')&=E_{1g}t''+E_{2g}t'\\&-\int_{t''}^{t'}[\mathbf{k}+\mathbf{A}(\tau)]^2/2d\tau-\int_{t'}^{\infty}[\mathbf{p}_1+\mathbf{A}(\tau)]^2/2d\tau\\&-\int_{t'}^{\infty}[\mathbf{p}_2+\mathbf{A}(\tau)]^2/2d\tau,\end{aligned} \tag{2}$$

and the form factors

$$V_{\mathbf{k}g}=\left\langle\psi_{\mathbf{k}}^{(V)}|V_1|\psi_g^{(1)}\right\rangle, \tag{3}$$

$$V_{\mathbf{p}_1\mathbf{p}_2,\mathbf{k}g}=\left\langle\psi_{\mathbf{p}_1}^{(V)}\psi_{\mathbf{p}_2}^{(V)}|V_{12}|\psi_{\mathbf{k}}^{(V)}\psi_g^{(2)}\right\rangle. \tag{4}$$

Taking into account depletion of the excited states, the transition amplitude of RESI process is

$$\begin{aligned}M^{\mathrm{RESI}}(\mathbf{p}_1,\mathbf{p}_2)=&\int_{-\infty}^{\infty}dt\int_{-\infty}^{t}dt'\int_{-\infty}^{t'}dt''\int d^3\mathbf{k}\\&\times e^{-\int_{t'}^{t}\gamma_j sin^2\omega\tau/2}V_{\mathbf{p}_2e}V_{\mathbf{p}_1e,\mathbf{k}g}V_{\mathbf{k}g}\\&\times e^{iS(\mathbf{p}_1,\mathbf{p}_2,\mathbf{k},t,t',t'')},\end{aligned} \tag{5}$$

with the action

$$\begin{aligned}S(\mathbf{p}_1,\mathbf{p}_2,\mathbf{k},t,t',t'')&=E_{1g}t''+E_{2g}t'+E_{2e}(t-t')\\&-\int_{t''}^{t'}[\mathbf{k}+\mathbf{A}(\tau)]^2/2d\tau-\int_{t'}^{\infty}[\mathbf{p}_1+\mathbf{A}(\tau)]^2/2d\tau\\&-\int_{t}^{\infty}[\mathbf{p}_2+\mathbf{A}(\tau)]^2/2d\tau,\end{aligned} \tag{6}$$

and the form factors

$$V_{\mathbf{k}g}=\left\langle\psi_{\mathbf{k}}^{(V)}|V_1|\psi_g^{(1)}\right\rangle, \tag{7}$$

$$V_{\mathbf{p}_1e,\mathbf{k}g}=\left\langle\psi_{\mathbf{p}_1}^{(V)}\psi_e^{(2)}|V_{12}|\psi_{\mathbf{k}}^{(V)}\psi_g^{(2)}\right\rangle, \tag{8}$$

$$V_{\mathbf{p}_2e}=\left\langle\psi_{\mathbf{p}_2}^{(V)}|V_2|\psi_e^{(2)}\right\rangle, \tag{9}$$

where $\psi_g^{(i)}$ is the ground state of the ith electron, $\psi_e^{(2)}$ is the excited state of the second electron, $\psi_{\mathbf{p}}^{(V)}$ is the Volkoff state with asymptotic momentum $\mathbf{p}$, V_i denotes the binding potential of the i th electron, and V_{12} is the interaction between the two electrons. The depletion rate of the excited state is approximately described as $\gamma_j \sin^2\omega\tau/2$ [19] calculated from a numerical solution of the time-dependent Schrödinger equation for each excited state.

In our calculation,

$$V_i=-\frac{Z_i^{\mathrm{eff}}}{r_i},\quad V_{12}=\frac{1}{|\mathbf{r}_1-\mathbf{r}_2|}, \tag{10}$$

where $Z_i^{\mathrm{eff}}=n\sqrt{2E_i}$ is the effective charge of the ith electron, n is the principal quantum number of the bound state, and E_i is the respective ionization potential of the ith electron. The trajectories are the solutions of the following saddle-point equations for the RII process:

$$[\mathbf{k}+\mathbf{A}(t'')]^2=-2E_{1g}, \tag{11}$$

$$[\mathbf{p}_1+\mathbf{A}(t')]^2+[\mathbf{p}_2+\mathbf{A}(t')]^2=[\mathbf{k}+\mathbf{A}(t')]^2-2E_{2g}, \tag{12}$$

$$\int_{t''}^{t'}[\mathbf{k}+\mathbf{A}(\tau)]d\tau=0, \tag{13}$$

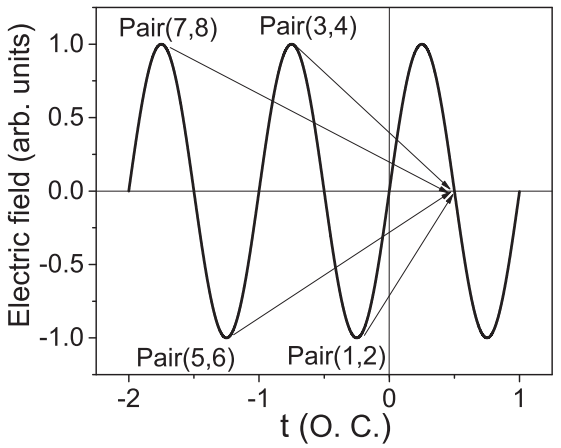

FIG. 1. Schematic representation of the electric field $\mathbf{E}(t)$ for a monochromatic field. The starts of the arrows indicate the approximate times around which the first electron tunnels, in case it returns at a crossing. The complex return and start times for the indicated pairs of orbits will have real parts in the vicinity of such times.

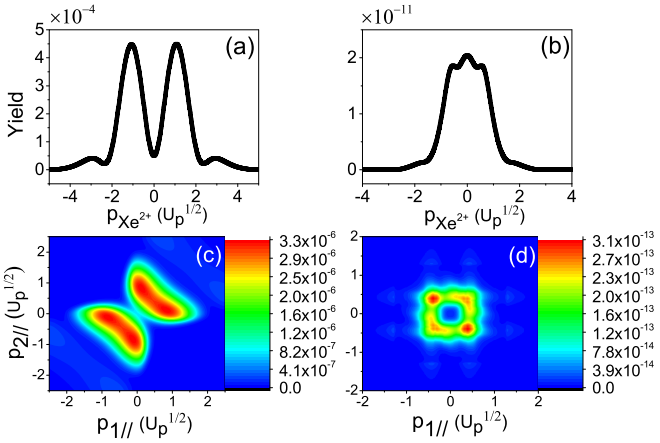

FIG. 2. (a), (b) Longitudinal momentum distribution of Xe^{2+}. (c), (d) Electron momentum correlation distribution for Xe ($E_{1g} = 0.4457$ a.u., $E_{2g} = 0.779$ a.u.). Panels (a) and (c) are for RII process, and panels (b) and (d) are for RESI process. The laser intensity is 2.5×10^{13} W/cm^2 and frequency $\omega = 0.018\,98$ a.u. (corresponding to wavelength $\lambda = 2400$ nm).

and for the RESI process

$$[\mathbf{k} + \mathbf{A}(t'')]^2 = -2E_{1g}, \tag{14}$$

$$[\mathbf{p}_1 + \mathbf{A}(t')]^2 = [\mathbf{k} + \mathbf{A}(t')]^2 - 2(E_{2g} - E_{2e}), \tag{15}$$

$$\int_{t''}^{t'} [\mathbf{k} + \mathbf{A}(\tau)]d\tau = 0, \tag{16}$$

$$[\mathbf{p}_2 + \mathbf{A}(t)]^2 = -2E_{2e}. \tag{17}$$

The orbit starts from the origin at the complex time t'' and the first electron rescatters at the time t'. The second electron is released at complex time t. We consider a monochromatic, linearly polarized field, for which

$$\mathbf{A}(t) = A_0 \cos(\omega t)\hat{\mathbf{e}}_z, \tag{18}$$

where A_0 is the amplitude of the vector potential, ω is the frequency, and $\hat{\mathbf{e}}_z$ denotes the polarization vector.

For the first electron, the solutions of saddle-point equations (11)–(13) and (14)–(16) are presented in pairs. In each pair, the two orbits are dubbed the short and long orbit corresponding to the shorter and longer travel times. Each cycle will then contain two pairs of orbits. In our calculation we restrict the real part of the return time in the interval $0 < t'_{Re} < T/2$, where t'_{Re} is the real part of t', and the tunneling time t'' may distribute in different half-cycles, as depicted in Fig. 1. Note that orbit 1 is the short orbit and orbit 2 is the long orbit in pair (1,2). Orbit 3 is the short orbit and orbit 4 is the long orbit in pair (3,4), and so on. The saddle-point approximation can only be applied when the saddle points are well separated, which is not the case near the boundary of the classically allowed region in momentum space. Hence, each pair of saddles in the same half cycle has to be treated in a uniform approximation [32]. In this paper, we will employ the standard saddle-point approximation to describe the contribution of individual orbit in one pair, and use the uniform approximation to describe the contribution of one pair as a whole. To demonstrate the interferences of different returning trajectories of the first electron, we will consider the four shortest pairs of trajectories, namely, pair (1, 2) to pair (7, 8). Meanwhile, for the second electron, we only consider the orbit with ionization time within half a cycle after the rescattering moment, which means we do not consider interference between ionization of the second electron at different optical cycles.

Then, we calculate the momentum correlation function by integrating over the transverse momenta,

$$W(p_{1\parallel}, p_{2\parallel}) = \int d^2p_{1\perp}d^2p_{2\perp}|M(\mathbf{p}_1, \mathbf{p}_2)|^2, \tag{19}$$

where $p_{i\parallel}$ and $p_{i\perp}$ denote the components of $\mathbf{p}_i$ parallel and perpendicular to the laser polarization axis, respectively.

If the contributions from different pairs of orbits are summed coherently or incoherently, the momentum correlation function are

$$W_{\rm coh}(p_{1\parallel}, p_{2\parallel}) = \int d^2p_{1\perp}d^2p_{2\perp}\left|\sum_c M_c(\mathbf{p}_1, \mathbf{p}_2)\right|^2, \tag{20}$$

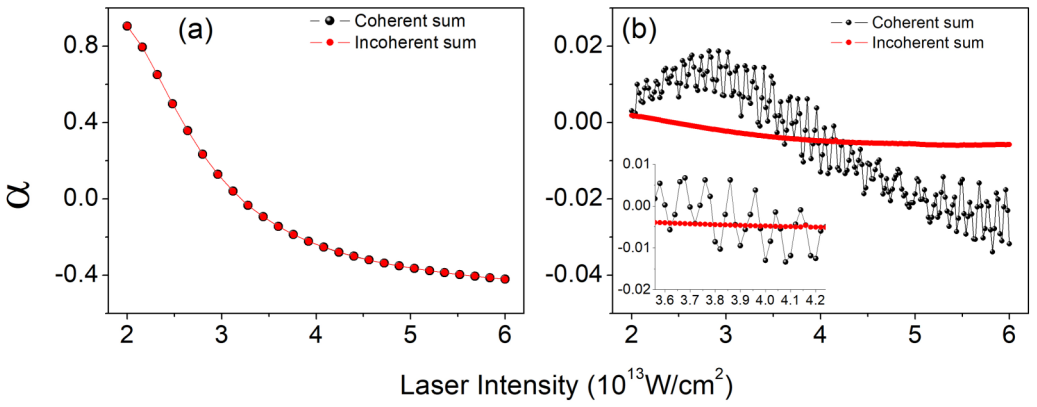

FIG. 3. The asymmetry parameter α of as a function of laser intensity. Panel (a) corresponds to the RII process with and without interference between the four shortest pairs of orbits for Xe. Panel (b) corresponds to the RESI process with both the interference between two ionic excitation channels of the second electron and between four pairs of returning orbits of the first electron are considered. The result with neither interference included is also presented for comparison.

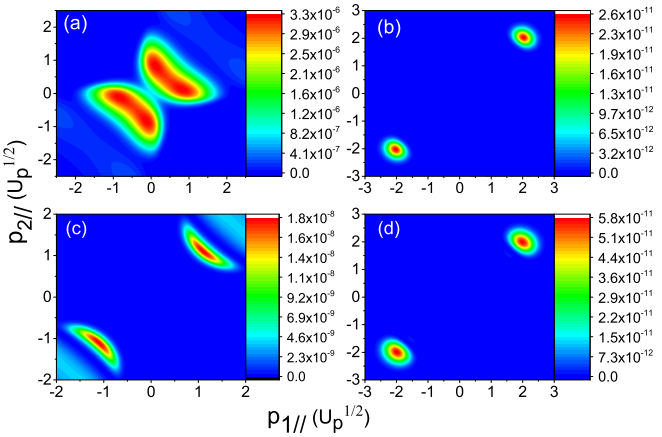

FIG. 4. Calculated electron momentum correlation distribution for different pairs of the first electron's returning quantum orbits in RII process. Panels (a)–(d) correspond to pair (1, 2), pair (3, 4), pair (5, 6), and pair (7, 8) of the first electron's returning orbits, respectively. The laser field has peak intensity 2.5×10^{13} W/cm^2.

and

$$W_{\text{incoh}}(p_{1\parallel}, p_{2\parallel}) = \int d^2p_{1\perp} d^2p_{2\perp} \sum_c |M_c(\mathbf{p}_1, \mathbf{p}_2)|^2, \quad (21)$$

respectively. The indices c refer to the different pairs of orbits.

Note that the electrons are indistinguishable and the monochromatic laser field is symmetrical in the sense of $\mathbf{A}(t + \frac{T}{2}) = -\mathbf{A}(t)$, so the below-stated arguments hold upon the exchange$(\mathbf{p}_1, \mathbf{p}_2) \leftrightarrow (\mathbf{p}_2, \mathbf{p}_1)$ and $(\mathbf{p}_1, \mathbf{p}_2) \leftrightarrow (-\mathbf{p}_1, -\mathbf{p}_2)$.

III. RESULTS AND DISCUSSIONS

For the laser parameters interested here (laser intensity $I > 2 \times 10^{13}$ W/cm^2 and wavelength $\lambda = 2400$ nm), the maximal energy of the first electron when it returns to the parent core exceeds the ionization potential of the second electron, so both RII and RESI processes may contribute to double ionization of Xe [23]. But the two-electron correlation corresponding to these two processes are very different. For example, as shown in Fig. 2, the longitudinal momentum distribution of Xe^{2+} for RII process exhibits a typical bimodal structure, and the momentum of the two electrons mainly distributes in quadrants 1 and 3. In contrast, for RESI process, the longitudinal momentum distribution of Xe^{2+} shows a peak at vanishing momentum, and the momentum of the two electrons mainly distributes in quadrants 2 and 4.

The asymmetry parameter defined as $\alpha = (Y_{1\&3} - Y_{2\&4})/(Y_{1\&3} + Y_{2\&4})$, where $Y_{1\&3}$ ($Y_{2\&4}$) denotes the yields of distributions in the first and third (second and fourth) quadrants, can be used to quantitatively depict the two-electron correlation. In Ref. [23], it is found that the measured laser intensity dependence of α for Xe at 2400 nm exhibit a behavior of fast oscillation. Applying the same laser parameters as in the measurement, we calculate the asymmetry parameters using Eqs. (1) and (5) corresponding to the RII process and the RESI process, respectively, as shown in Fig. 3. The contributions of four shortest pairs of first electron's returning orbits are summed coherently or incoherently to identify the effect of inference. For the RESI process, in addition to the interference between different returning orbits of the first electron, interference between different excitation channels of the second electron is also included.

For RII process [Fig. 3(a)], the resulting curve in the case of coherent sum remarkably coincides with that in the case of incoherent sum, which shows a smooth decreasing trend. This indicates that the effect of interference among four shortest pairs of first electron's returning orbits is negligible. This can be understood as follows: First, the contributions from pair (3,4), pair (5,6), and pair (7,8) are too small to interfere with par(1,2). As shown in Fig. 4, the maximum of momentum distribution for pair (1,2) is 127 000 times of that for pair (3,4),

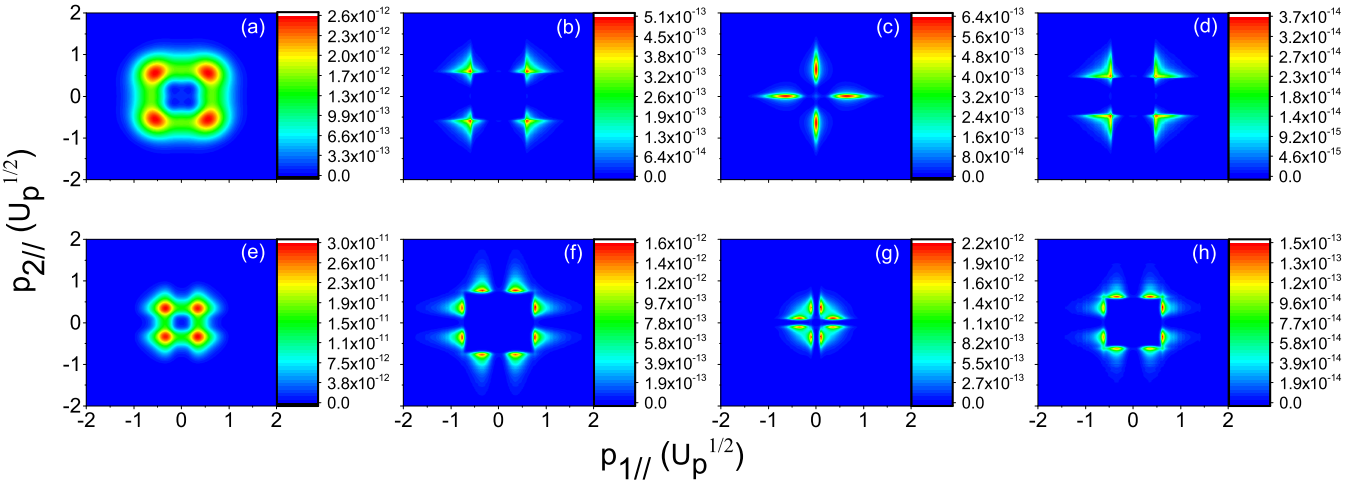

FIG. 5. Calculated electron momentum correlation distributions of single component in each pair of first electron's returning quantum orbits for Xe. Panels (a)–(d) correspond to orbit 2 in pair (1, 2), orbit 3 in pair (3, 4), orbit 6 in pair (5, 6), and orbit 7 in pair (7, 8), respectively, with ionic state $5p^45d$ ($E_{2e} = 0.345$ a.u.) of the second electron. Panels (e)–(h) correspond to orbit 2 in pair (1, 2), orbit 3 in pair (3, 4), orbit 6 in pair (5, 6), and orbit 7 in pair (7, 8), respectively, with ionic state $5p^46s$ ($E_{2e} = 0.19$ a.u.) of the second electron. The laser field has intensity $I = 4.0 \times 10^{13}$ W/cm^2 and frequency $\omega = 0.018\,98$ a.u. (corresponding to wavelength $\lambda = 2400$ nm).

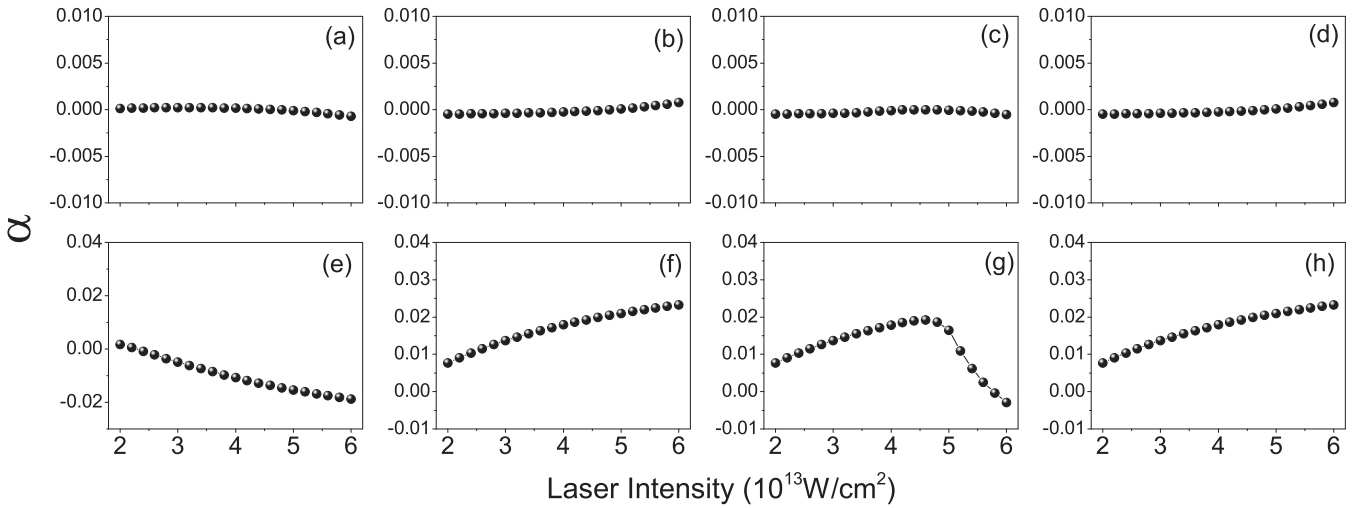

FIG. 6. The asymmetry parameter α as a function of laser intensity for single component in each pair of first electron's returning quantum orbits for Xe. Panels (a)–(d) correspond to orbit 2 in pair (1, 2), orbit 3 in pair (3, 4), orbit 6 in pair (5, 6), and orbit 7 in pair (7, 8), respectively, with the second electron ionic state $5p^45d$. Panels (e)–(h) correspond to orbit 2 in pair (1, 2), orbit 3 in pair (3, 4), orbit 6 in pair (5, 6), and orbit 7 in pair (7, 8), respectively, with the second electron ionic state $5p^46s$.

180 times of that for pair (5,6) and 56900 times of that for pair (7,8). Second, since the return energy is different for different pairs, the final momentum of the first electron for different pairs are also different. As shown in Fig. 4, the momentum distributions for different pairs are localized in different areas and there is little overlap between them, so they can hardly interference with each other.

Whereas for RESI process in Fig. 3(b), the asymmetry parameter shows a series of quickly oscillations with a period about 1.0 TW/cm^2. If not including the interference between different pairs and that between different excitation channels, the oscillation disappears. To identify the interference between which specific orbits leading to the fast oscillations, we will systematically analyze the effects different orbits in the following.

Figure 5 shows the electron momentum correlation distributions corresponding to each single one of the returning orbits at different ionic excitation channels of the second electron. Note that only orbits 2, 3, 6, and 7 are presented, since the other orbits 1, 4, 5, and 8 will generate an exponentially increasing contribution outside of the classically allowed region which are not physical. The shape of the momentum distribution depends both on the returning orbits of the first electron and the ionic excitation channel of the second electron. If the second electron is excited to the $5p^45d$ state and then ionized, we observe four spots in the vicinity of $p_{1\parallel} = \pm p_{2\parallel}$ for orbits 2, 3, and 7, while the maximum of the distribution merge along the $p_{n\parallel}$ axis and the cross-shaped distributions are observed for orbit 6. If one assumes that the second electron is ionized through excited state $5p^46s$, there

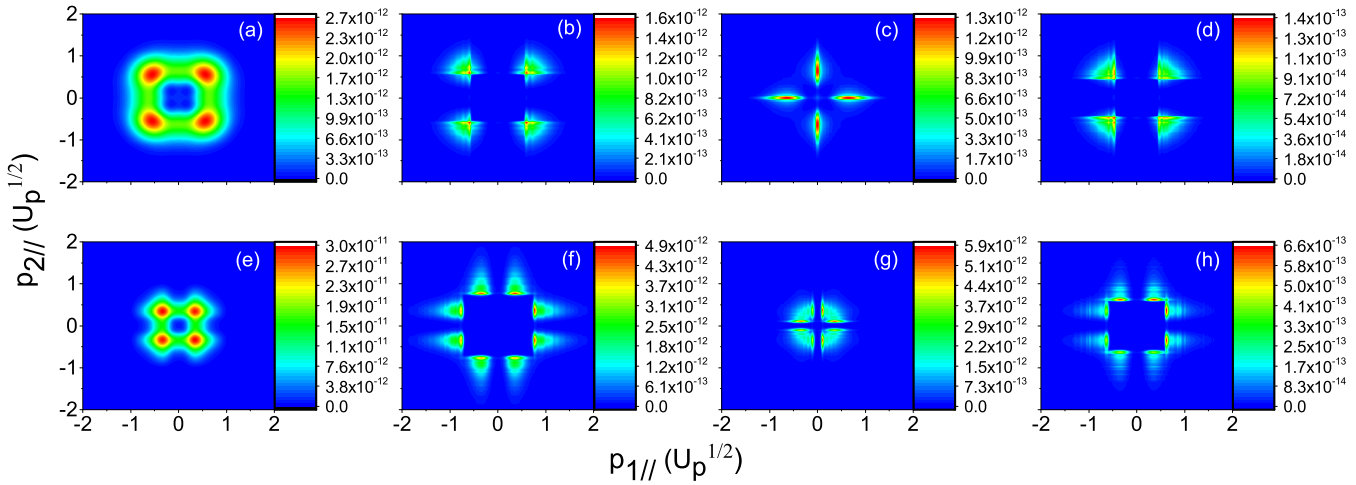

FIG. 7. Calculated electron momentum correlation distributions in terms of the interference between the two components in each pair of the first electron's returning orbits for Xe. Panels (a)–(d) correspond to pair (1, 2), pair (3, 4), pair (5, 6), and pair (7, 8), respectively, with the second electron ionic state $5p^45d$. Panels (e)–(h) correspond to pair (1, 2), pair (3, 4), pair (5, 6), and pair (7, 8), respectively, with the second electron ionic state $5p^46s$. The parameters of laser field are the same as that of Fig. 5.

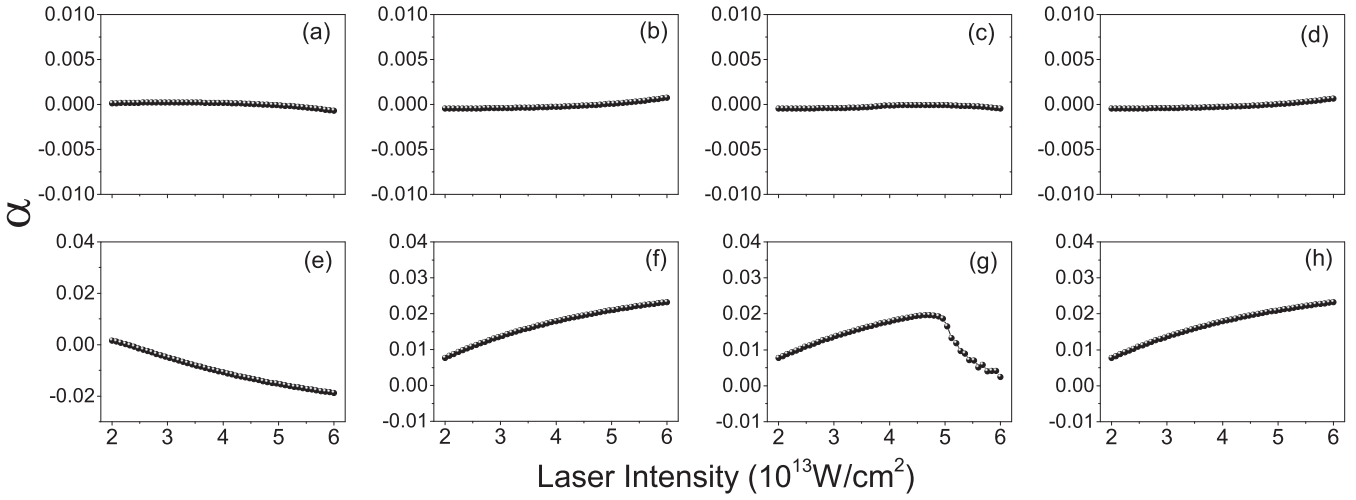

FIG. 8. The asymmetry parameter α as a function of laser intensity in terms of the pairs of the first electron's returning quantum trajectories. Panels (a)–(d) correspond to pair (1, 2), pair (3, 4), pair (5, 6), and pair (7, 8), respectively, with the second electron ionic state $5p^45d$. Panels (e)–(h) correspond to pair (1, 2), pair (3, 4), pair (5, 6), and pair (7, 8), respectively, with the second electron ionic state $5p^46s$.

are also four spots in the vicinity of $p_{1\parallel} = \pm p_{2\parallel}$ for orbit 2, while a splitting is found in their distribution peak value for orbits 3, 6, and 7, respectively. It should be noted that the excited state $5p^45d$ is a pure $5d$ state, while the state $5p^46s$ contains about 10% $6d$ admixture in addition to the dominant $6s$ component.

The magnitude of the distribution probability varies with different orbits. When the second electron is ionized through excited state $5p^45d$, the maximum of momentum distribution for orbit 2 is four times of that for orbit 6, and five times of that for orbit 3. When ionized through excited state $5p^46s$, it turns out to be 14 times and 19 times, respectively. Therefore, orbit 2 plays a dominant role among orbits 2, 3, 6, 7. The second-most important contribution is from orbit 6, which is larger than that from orbit 3. Orbit 7 has the smallest contribution. This is due to that the kinetic energy upon collision of the first electron for orbits 2 or 6 is much higher than that for orbits 3 or 7, and therefore is more likely to promote the second electron to an excited state.

Figure 6 shows the intensity dependence of α for each single orbit. In general, all the curves are very smooth. When the second electron is excited to $5p^45d$ ionic state, the asymmetry parameter of orbits 2, 3, 6, and 7 are all around zero. This means that electron pairs are inclined to evenly distribute in all four quadrants. When the second electron is excited to the $5p^46s$ ionic state, the asymmetry parameter of orbit 2 shows a decreasing trend and turns to be negative, indicating that back to back emission mechanism dominates for orbits whose returning time are within one laser cycle. The asymmetry parameter of both orbits 3 and 7 show an increasing trend and are positive. The asymmetry parameter of orbit 6 first increases and then decreases, holding positive for the most part with increase of laser intensity. Therefore, the two electrons are apt to perform a side by side emission with returning orbits 3, 6, 7, whose returning time are beyond one laser cycle.

In Figs. 7 and 8, we present the electron momentum correlation distributions and intensity dependence of α after considering the interference between two quantum orbits in each pair (intrapair interference). The results are calculated

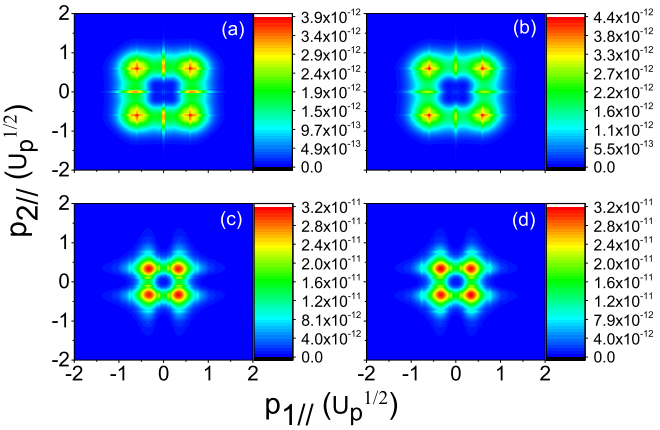

FIG. 9. Electron momentum correlation distribution with (first column) and without (second column) interference between the four shortest pairs of orbits with different ionic excitation channels of the second electron. (a), (b) The second electron ionic state $5p^45d$; (c), (d) the second electron ionic state $5p^46s$. The parameters of laser field are the same as that of Fig. 5.

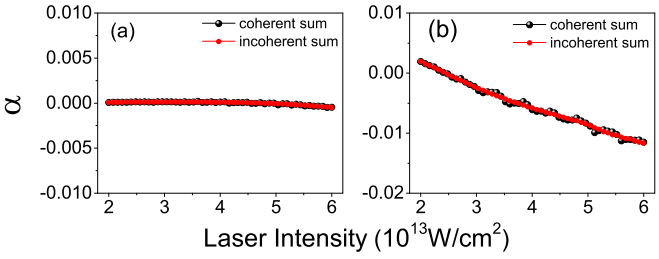

FIG. 10. The asymmetry parameter α as a function of laser intensity for RESI process with and without interference between the four shortest pairs of orbits for the second electron ionic states. (a) $5p^45d$; (b) $5p^46s$.

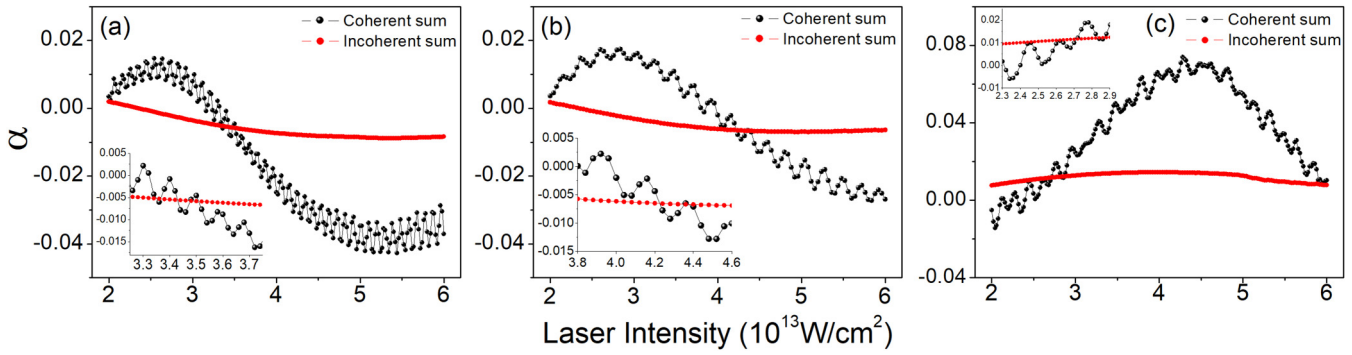

FIG. 11. The intensity dependence of asymmetry parameter α (a) considering interferences between pair (1,2) and pair (5,6) in both $5p^45d$ and $5p^46s$, (b) considering interferences between pair (1,2) and pair (3,4) in both $5p^45d$ and $5p^46s$, and (c) considering interferences between pair (3,4) and pair (5,6) in both $5p^45d$ and $5p^46s$.

based on the uniform approximation. By comparing Figs. 7 and 8 with Figs. 5 and 6, we can extract the effect of interference between two orbits in each pair. After coherently adding the other orbit in each pair, the shapes of the momentum distributions only change in details, but the magnitudes of the momentum distribution vary obviously. Specifically, the results for pair (1,2) are almost the same as that for orbit 2 alone, which means that the contribution from orbit 1 is too small to interfere with orbit 2. But this is not the case for other pairs (3, 4), (5, 6) and (7, 8), in which the two orbits make similar contributions. As for intensity dependence of asymmetry parameter, the effect of intrapair interference effect appears to be negligible, which can be inferred by comparing Fig. 8 with Fig. 6. This is because the intrapair interference does not break the symmetry of momentum correlation distribution with respect to $p_{2\parallel} = 0$.

Next, we coherently sum the contributions from different pairs of returning orbits, as shown in Fig. 9. For comparison, we also present results of incoherent sum of different pairs of orbits. Since pair (1, 2) has dominant contribution among all pairs of orbits, the resulting distribution pattern made up by the coherent sum has remarkably similarity with that of incoherent sum. So the interference effect manifests itself only in detail of the distribution, for example, it enhances the maxima of the distribution probability along the $p_{n\parallel}$ axis in Fig. 9(a) compared with Fig. 9(b). Moreover, the interference also affects the intensity dependence of asymmetry parameter, as shown in Fig. 10, which presents oscillation in both cases of the two excitation channels, but the amplitude is too small compared with the oscillation in Fig. 3(b). This indicates that the region and magnitude of momentum distributions do not match so well. Therefore, the fast oscillation of the laser dependence of asymmetry parameter in Fig. 3(b) is not the result of interferences between different rescattering orbits in each excitation channel.

Then the fast oscillation in Fig. 3(b) can only be attributed to mixed interpair interference among the two excitation channels, i.e., the interference between one pair in $5p^45d$ and another pair in $5p^46s$. In the following we seek to identify the two specific pairs whose interference contributes dominantly to the fast oscillation in Fig. 3(b). Since pair (7,8) makes almost negligible contribution, we mainly focus on interferences between pairs (1,2), (3,4), and (5,6) among the two excitation channels. First, we present the calculated asymmetry parameter including only two pairs of orbits in the two excitation channels in Fig. 11. We find that the mixed interference in different combinations can all induce fast oscillation, but the period is different. The mixed interference among pairs (1,2) and (5,6) in the two excitation channels [Fig. 11(a)] shows a similar fast oscillation with a period of 1.0 TW/cm^2 as that in Fig. 3(b). The period of oscillations corresponding to pairs (1,2) and (3,4) in Fig. 11(b) is about 2.4 TW/cm^2, and that corresponding to pairs (3,4) and (5,6) in Fig. 11(c) is 1.6 TW/cm^2. Therefore, we can conclude that the oscillations

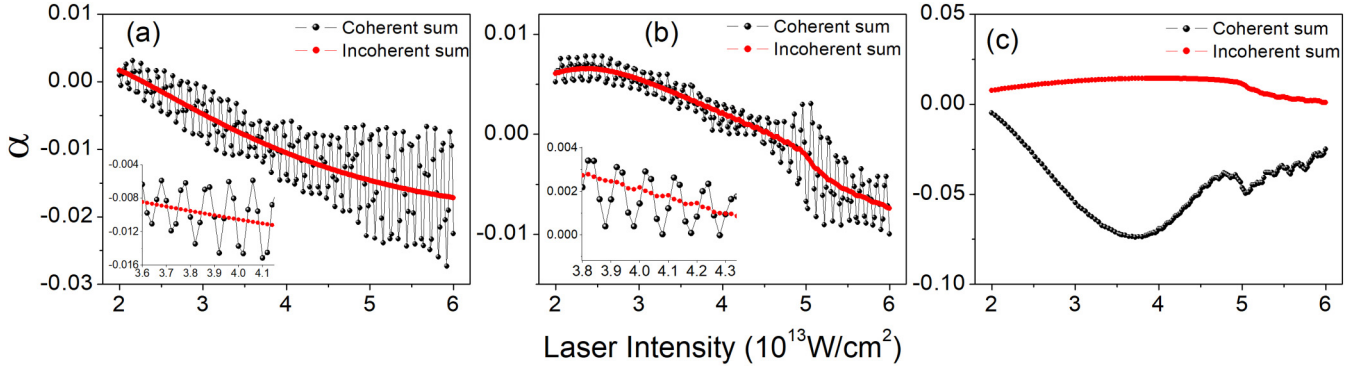

FIG. 12. Laser intensity dependence of the asymmetry parameter α (a) considering interference between pair (5,6) in $5p^45d$ and pair (1,2) in $5p^46s$, (b) pair (1,2) in $5p^45d$ and pair (5,6) in $5p^46s$, (c) and pair (5,6) in $5p^45d$ and pair (5,6) in $5p^46s$.

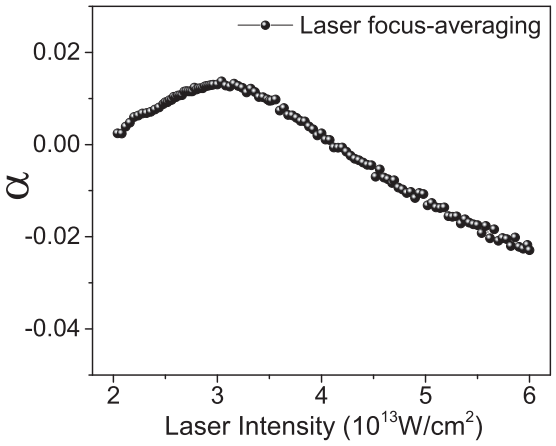

FIG. 13. Laser intensity dependence of the asymmetry parameter α considering interferences between all the four pairs of returning orbits in excitation channels of $5p^4 5d$ and $5p^4 6s$ after performing laser focus averaging.

of asymmetry parameter with respect to laser intensity in Fig. 3(b) mainly result from mixed interference between pair (1,2) and pair (5,6) in the two excitation channels.

Next we further determine which pair between the two in each excitation channel causes the interference by checking all the possible combinations. Note that the interference between the two pairs of (1,2) in each excitation channel has been reported in Ref. [23], which shows that this interference only shapes the general envelope of laser intensity dependence of asymmetry parameter but does not generate the fast oscillation. Therefore, we only present the results of the other three cases in Fig. 12. It is found that both the mixed interference between pair (5,6) in $5p^4 5d$ and pair (1,2) in $5p^4 6s$ [Fig. 13(a)], and that between pair (1,2) in $5p^4 5d$ and pair (5,6) in $5p^4 6s$ can produce obvious fast oscillations with a period of 1.0 TW/cm^2. However, for the interference between two pairs of (5,6) from each excitation channel, only smooth variation similar to the case of two pairs of (1,2) can be found. Therefore, the fast oscillations in Fig. 3(b) can be attributed to the mixed interference between pair (1,2) and pair (5,6) but in different excitation channels.

From Figs. 12(a) and 12(b), the obtained oscillation of asymmetry parameter shows the equal-spacing interference fringes, which indicates that the phase of electrons linearly scales with the laser intensity. In the following, we discuss the relation between the electron phase and the laser intensity from an analytical view via the saddle-point approximation. The electron phase is represented by the corresponding actions $S(\mathbf{p}_1, \mathbf{p}_2, \mathbf{k}, t, t', t'')$. The phase difference between the action of pair (5,6) and pair (1,2) of the first electron's rescattering orbit in different excitation channels is

$$\Delta S = S_{(5,6)}(\mathbf{p}_1, \mathbf{p}_2, \mathbf{k}_2, t_2, t_2', t_2'') - S_{(1,2)}(\mathbf{p}_1, \mathbf{p}_2, \mathbf{k}_1, t_1, t_1', t_1''), \tag{22}$$

where t_1'' (t_2'') represents the tunneling time of the first electron for pair (1,2) [pair (5,6)], t_1' (t_2') is the rescattering time of the first electron for pair (1,2) [pair (5,6)], t_1 (t_2) represents the tunneling time of the second electron for pair (1,2) [pair (5,6)].

For pair (1,2), the tunneling time t_1'' is approximately at the field crest and rescattering time t_1' is approximately at the subsequent field crossing, as shown in Fig. 1, so we have $t_1' - t_1'' \approx \frac{3\pi}{2\omega}$, $\sin(\omega t_1'') \approx -1$, and $\sin(\omega t_1') \approx 0$. For pair (5,6), if its rescattering time is fixed near that of pair (1,2), i.e., $t_2' \approx t_1'$, the tunneling time has the relation $t_2'' \approx t_1'' - \frac{2\pi}{\omega}$. The tunneling times of the second electron for the two pairs can be set as equal, i.e., $t_2 = t_1$. As a result,

$$\begin{aligned}\Delta S &= S_{(5,6)} - S_{(1,2)} \\ &= E_{1g}(t_2'' - t_1'') + E_{2e2}(t_2 - t_2') - E_{2e1}(t_1 - t_1') \\ &\quad + U_p\left(\frac{4}{7\pi\omega} - \frac{4}{3\pi\omega} - \frac{2\pi}{\omega}\right),\end{aligned} \tag{23}$$

where E_{2ei} $(i = 1, 2)$ denotes the ionization potential of the second electron's excited state. We can infer from the above results that α linearly scales with U_p, which is proportional to the laser intensity. By setting $\Delta S_2 - \Delta S_1 = -2\pi$, we can receive $\Delta U_p = U_{p_2} - U_{p_1} = 0.018$ a.u., corresponding to the period as $\Delta I = I_2 - I_1 = 0.9$ TW/cm^2, which agrees well with the results in Fig. 12.

Finally, we perform laser focus averaging on electron momentum correlation distribution considering both the interference between two ionic excitation channels of the second electron and between four pairs of returning orbits of the first electron. Unfortunately, fast oscillation on the laser intensity dependence of asymmetry parameter disappears, as shown in Fig. 13. This may be because the period of the oscillation in Fig. 3(b) is too small. However, the above results is based on SFA, so the effect of Coulomb field between the ionized electron and the residual ion is not included. According to Ref. [33], the rescattering orbits will be significantly affected by the Coulomb field, including the relative contribution between different pairs, the spatial trajectory, as well as the phase. Therefore, if taking the Coulomb field into account, the amplitude and period of the oscillation will change, and the oscillation may survive after focus averaging.

IV. CONCLUSIONS

In this paper, we utilize SFA to systematically investigate the interference effect between rescattering electrons' returning orbits in the RESI process. We find that the intrapair interference is negligible, but the mixed interference between different pairs of returning orbits in different excitation channels is prominent, which induces fast oscillations with constant period in the laser-intensity dependence of the asymmetry parameter. However, it is found that the oscillation disappears when laser focus averaging is performed due to its rather small period. More sophisticated models accounting for effects, e.g., ion-electron Coulomb interaction and dressing of the excited states, still need to be developed to explain the experimental observation.

ACKNOWLEDGMENTS

This work is supported by the National Key R&D Program of China (Grants No. 2019YFA0307700 and No. 2016YFA0401100) and NNSFC (No. 11874246).

[1] A. l'Huillier, L. A. Lompre, G. Mainfray, and C. Manus, Phys. Rev. A **27**, 2503 (1983).

[2] Th. Weber, M. Weckenbrock, A. Staudte, L. Spielberger, O. Jagutzki, V. Mergel, F. Afaneh, G. Urbasch, M. Vollmer, H. Giessen, and R. Dörner, Phys. Rev. Lett. **84**, 443 (2000).

[3] R. Moshammer, B. Feuerstein, W. Schmitt, A. Dorn, C. D. Schröter, J. Ullrich, H. Rottke, C. Trump, M. Wittmann, G. Korn, K. Hoffmann, and W. Sandner, Phys. Rev. Lett. **84**, 447 (2000).

[4] Th. Weber, H. Giessen, M. Weckenbrock, G. Urbasch, A. Staudte, L. Spielberger, O. Jagutzki, V. Mergel, M. Vollmer, and R. Dörner, Nature (London) **405**, 658 (2000).

[5] A. Becker and F. H. M. Faisal, Phys. Rev. Lett. **84**, 3546 (2000).

[6] J. Chen, J. Liu, L. B. Fu, and W. M. Zheng, Phys. Rev. A **63**, 011404(R) (2000).

[7] A. Staudte, C. Ruiz, M. Schöffler, S. Schössler, D. Zeidler, Th. Weber, M. Meckel, D. M. Villeneuve, P. B. Corkum, A. Becker, and R. Dörner, Phys. Rev. Lett. **99**, 263002 (2007).

[8] A. Rudenko, V. L. B. de Jesus, Th. Ergler, K. Zrost, B. Feuerstein, C. D. Schröter, R. Moshammer, and J. Ullrich, Phys. Rev. Lett. **99**, 263003 (2007).

[9] Y. Liu, S. Tschuch, A. Rudenko, M. Dürr, M. Siegel, U. Morgner, R. Moshammer, and J. Ullrich, Phys. Rev. Lett. **101**, 053001 (2008).

[10] B. Bergues, M. Kübel, N. Johnson, B. Fischer, N. Camus, K. Betsch, O. Herrwerth, A. Senftleben, A. Sayler, T. Rathje *et al.*, Nat. Commun. **3**, 813 (2012).

[11] K. J. Schafer, Baorui Yang, L. F. DiMauro, and K. C. Kulander, Phys. Rev. Lett. **70**, 1599 (1993).

[12] P. B. Corkum, Phys. Rev. Lett. **71**, 1994 (1993).

[13] J. Ullrich, R. Moshammer, A. Dorn, R. Dörner, L. Ph. H. Schmidt, and H. Schmidt-Böcking, Rep. Prog. Phys. **66**, 1463 (2003).

[14] W. Becker, X. J. Liu, P. J. Ho, and J. H. Eberly, Rev. Mod. Phys. **84**, 1011 (2012).

[15] B. Feuerstein, R. Moshammer, D. Fischer, A. Dorn, C. D. Schröter, J. Deipenwisch, J. R. Crespo Lopez-Urrutia, C. Höhr, P. Neumayer, J. Ullrich *et al.*, Phys. Rev. Lett. **87**, 043003 (2001).

[16] E. Eremina, X. Liu, H. Rottke, W. Sandner, A. Dreischuh, F. Lindner, F. Grasbon, G. G. Paulus, H. Walther, R. Moshammer, B. Feuerstein, and J. Ullrich, J. Phys. B: At., Mol. Opt. Phys. **36**, 3269 (2003).

[17] T. Shaaran, M. T. Nygren, and C. Figueira de Morisson Faria, Phys. Rev. A **81**, 063413 (2010).

[18] B. B. Wang, Y. C. Guo, J. Chen, Z. C. Yan, and P. M. Fu, Phys. Rev. A **85**, 023402 (2012).

[19] X. L. Hao, J. Chen, W. D. Li, B. Wang, X. Wang, and W. Becker, Phys. Rev. Lett. **112**, 073002 (2014).

[20] T. Shaaran, C. Figueira de Morisson Faria, and H. Schomerus, Phys. Rev. A **85**, 023423 (2012).

[21] A. S. Maxwell and C. Figueira de Morisson Faria, Phys. Rev. A **92**, 023421 (2015).

[22] A. S. Maxwell and C. Figueira de Morisson Faria, Phys. Rev. Lett. **116**, 143001 (2016).

[23] W. Quan, X. L. Hao, Y. L. Wang, Y. J. Chen, S. G. Yu, S. P. Xu, Z. L. Xiao, R. P. Sun, X. Y. Lai, S. L. Hu *et al.*, Phys. Rev. A **96**, 032511 (2017).

[24] M. P. Hertlein, P. H. Bucksbaum, and H. G. Muller, J. Phys. B: At., Mol. Opt. Phys. **30**, L197 (1997).

[25] P. Hansch, M. A. Walker, and L. D. Van Woerkom, Phys. Rev. A **55**, R2535(R) (1997).

[26] R. Kopold and W. Becker, J. Phys. B: At., Mol. Opt. Phys. **32**, L419 (1999).

[27] G. G. Paulus, F. Grasbon, H. Walther, R. Kopold, and W. Becker, Phys. Rev. A **64**, 021401(R) (2001).

[28] W. Quan, X. Y. Lai, Y. J. Chen, C. L. Wang, Z. L. Hu, X. J. Liu, X. L. Hao, J. Chen, E. Hasović, M. Busuladžić, W. Becker, and D. B. Milošević, Phys. Rev. A **88**, 021401(R) (2013).

[29] C. Wang, M. Okunishi, X. Hao, Y. Ito, J. Chen, Y. Yang, R. R. Lucchese, M. Zhang, B. Yan, W. D. Li, D. Ding, and K. Ueda, Phys. Rev. A **93**, 043422 (2016).

[30] M. Bellini, C. Lyngå, A. Tozzi, M. B. Gaarde, T. W. Hänsch, A. L'Huillier, and C.-G. Wahlström, Phys. Rev. Lett. **81**, 297 (1998).

[31] S. V. Popruzhenko, P. A. Korneev, S. P. Goreslavski, and W. Becker, Phys. Rev. Lett. **89**, 023001 (2002).

[32] C. Figueira de Morisson Faria, H. Schomerus, and W. Becker, Phys. Rev. A **66**, 043413 (2002).

[33] X. L. Hao, Y. X. Bai, X. Y. Zhao, C. Li, J. Y. Zhang, J. L. Wang, W. D. Li, C. L. Wang, W. Quan, X. J. Liu *et al.*, Phys. Rev. A **101**, 051401(R) (2020).